

Supplementary Information for

Energetics of the exchangeable quinone, Q_B , in Photosystem II

Sven De Causmaecker^a, Jeffrey S. Douglass^a, Andrea Fantuzzi^a, Wolfgang Nitschke^b, and A. William Rutherford^{a1}

Corresponding Author: A.W. Rutherford, Department of Life Sciences, Sir Ernst Chain Building, Imperial College London, SW7 2AZ, UK, Tel + 44 2075945329,

E-mail: a.rutherford@imperial.ac.uk;

This PDF file includes:

Supplementary text

Figs. S1 to S15

Tables S1 to S2

References for SI reference citations

Supplemental Information

PSII purification:

T. elongatus cells were grown in DTN medium (1) in 5 l Erlenmeyer flasks (2 l culture) in a rotary shaker (120 rpm) at 45 °C under continuous illumination from fluorescent white lamps ($\approx 80 \mu\text{mol}$ of photons $\text{m}^{-2} \text{s}^{-1}$). Typically, 18 l of cell culture were grown until $\text{OD}_{750}=0.6$. After harvesting by filtration with a Sartocon Hydrosart Microfiltration Cassette (0.2 μm ; Sartorius Stedim UK Limited, Epsom, UK), the cells were centrifuged (11,280 g, 10 min) and washed once with buffer 1 (40 mM MES, 2.5 mM MgCl_2 , 2.5 mM CaCl_2 , 10% glycerol, 1 M betaine, 10 mM NaHCO_3 , pH 6.5) and re-suspended in the same buffer, containing 0.2% (w/v) bovine serum albumin, 1 mM benzamide, 50 $\mu\text{g ml}^{-1}$ DNase I and protease inhibitor cocktail (Cat. number 05 056 489 001; Roche, Basel, Switzerland) added to a chlorophyll (Chl) concentration of $\approx 1.5 \text{ mg (Chl) ml}^{-1}$. The cells were ruptured by being passed twice through a high pressure (20 kpsi) cell disruption system (Constant Systems Ltd., Northants, UK). All subsequent steps were carried out in dim green light at 4 °C. Unbroken cells were removed by centrifugation (1500 g, 5 min, 4 °C). Thylakoids (1 mg (Chl) ml^{-1} final concentration in buffer 1) were treated with 0.8% (w/v) *n*-dodecyl- β -maltoside (β -DM, Biomol, Germany). After brief (<10 min) and gentle mixing, the suspension was centrifuged (60 min, 185000 g) to remove the non-solubilized material. Then, the supernatant was mixed with an equal volume of Probond Ni-resin (Invitrogen, Netherlands) that had been pre-equilibrated with buffer 2 (buffer 1 + 15 mM imidazole, 0.03% (w/v) β -DM) and applied to a column. The resin was washed with buffer 2 until the OD value of the eluate at $\approx 670 \text{ nm}$ decreased below 0.05. Then, PSII core complexes were eluted with buffer 3 (buffer 1 + 300 mM imidazole, 0.06% (w/v) β -DM, pH adjusted to 6.5 by adding concentrated HCl). The eluate was concentrated and washed using centrifugal filters (100 kDa Amicon Ultra-15, Millipore-Merck, Germany). PSII core complexes were re-suspended either in buffer 1 or in titration buffer (40 mM MOPS, 2.5 mM MgCl_2 , 2.5 mM CaCl_2 , 10% glycerol, 1 M betaine, 10 mM NaHCO_3 , pH 7) at a Chl concentration of 1–1.5 mg (Chl) ml^{-1} and stored in liquid N_2 until use. The estimate of Chl concentration was done by extracting the chlorophyll with methanol and by using an extinction coefficient of 79.95 $\text{mg}^{-1} \text{ ml cm}^{-1}$ at 665 nm (2).

Oxygen evolution activity of PSII samples was measured in buffer 1 supplemented with 0.5 mM 2,6-dichloro-*p*-benzoquinone (DCBQ) and 1 mM potassium ferricyanide (FeCN) at 2.5–10 $\mu\text{g (Chl) ml}^{-1}$ of PSII using a Clark-type electrode (Oxygraph, Hansatech Instruments

Limited, UK) at 25 °C under saturating red light ($>10,000 \mu\text{mol m}^{-2} \text{s}^{-1}$). The oxygen evolution activity was typically $2500\text{--}3500 \mu\text{mol (O}_2\text{) mg (Chl)}^{-1}$.

Analysis of EPR redox titrations

The peak height of each peak was evaluated using Matlab R2018 script. The minima left and right of the peak are used to determine a baseline from which the peak height at the maximum is determined (exemplified in Fig S1 A for the $g \approx 2$ signal and B for the $g = 1.66$ signal).

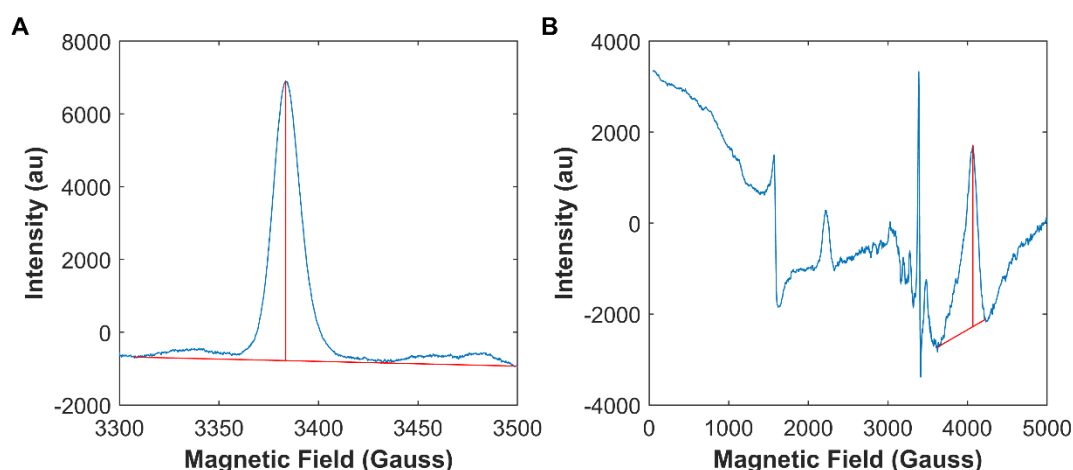


Figure S1 Examples of the data analysis for both EPR signals used to monitor Q_B^- using a Matlab script.

To obtain the redox potentials of the two couples $\text{Q}_\text{B}/\text{Q}_\text{B}^{\bullet-}$ and $\text{Q}_\text{B}^{\bullet-}/\text{Q}_\text{BH}_2$ the experimental data were fitted using the following expression.

$$[I] = \frac{[S]}{1 + 10^{(E - E_m - \frac{\Delta E}{2}) \frac{F}{RT}} + 10^{(E_m - E - \frac{\Delta E}{2}) \frac{F}{RT}}} \quad \text{Eq. S1}$$

Here [I] is defined as the observed concentration of the intermediate semiquinone. [S] is the total quinone concentration. The parameters

$$E_m = (E1 + E2)/2 \quad \text{Eq. S2}$$

and

$$\Delta E = E1 - E2 \quad \text{Eq. S3}$$

are used in the formula, since these determine the curve (ΔE determines shape and width/height of the curve, E_m determines the position of the curve). Whilst technically a formula using E1 and E2 as separate parameters could also be used for the fitting (see (3)), this would be incorrect since one then would derive different confidence intervals of the fit for E1 and E2. The whole bell curve, however, is dependent equally on both E1 and E2 and

therefore the uncertainty in the fit applies equally to E1 and E2.¹ Different confidence intervals with regards to position and shape of curve on the other hand are to be expected. For more details on how these relationships are derived see Michaelis (4) or Nitschke (5).

Total Q_B estimate

Equation S1 shows that if the total Q_B concentration is known (i.e. signal size for 100% $Q_B^{\bullet-}$), ΔE can be calculated from the concentration of the intermediate when $E = E_{max}$. We therefore estimated the signal size of the $Q_B^{\bullet-}Fe^{2+}$ signal if present in 100% of the centers ([S] in eq S1) as described on Page 6. The $Q_B^{\bullet-}Fe^{2+}$ signal was measured in a dark-adapted PSII sample prior to the addition of mediators. Then the sample was illuminated at 77 K, thawed in darkness and the $Q_B^{\bullet-}Fe^{2+}$ signal was measured again. Figure S1 C shows the $Q_B^{\bullet-}Fe^{2+}$ signals before (red) and after (dark red) 77 K illumination and thawing in darkness. The blue curve is the addition of the two signals and the black curve is the maximum signal observed in the subsequent titration of the same sample. The observed maximum signal in the titration ([I] at $E = E_m$) equals 59 % of the calculated maximum. Using equation S1 this can be translated directly to a $\Delta E \approx 54$ mV without the necessity of fitting (or even doing) the full titration.

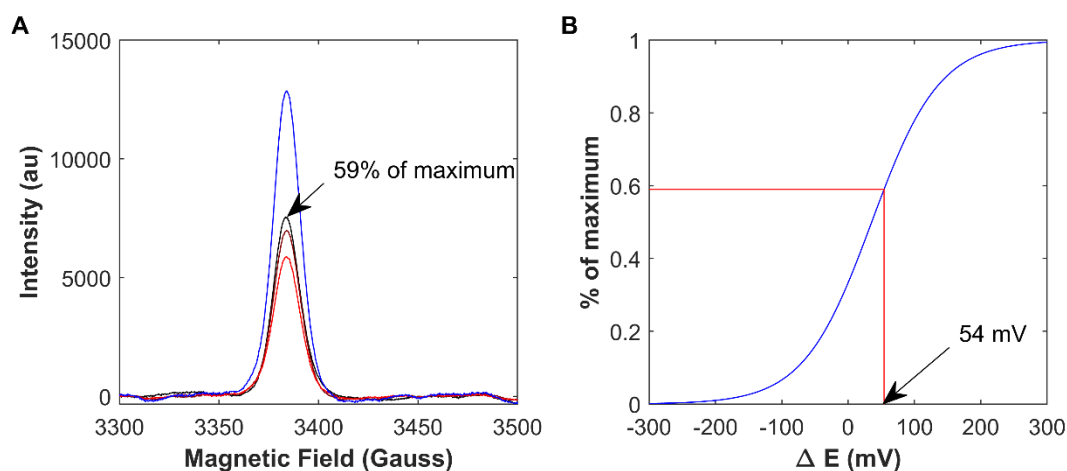


Figure S2 **A** Red: $Q_B^{\bullet-}Fe^{2+}$ signal in the dark; Dark red: $Q_B^{\bullet-}Fe^{2+}$ signal after 77K illumination and thawing in darkness; Blue: Addition of the previous two; Black: largest observed signal in the following titration. **B** Plot of the relative size of the bell curve in relation to the total amount of Q_B vs ΔE

¹ This symmetry also means that, in principal, both E1 and E2 can be determined even if only half the bell curve where reversibly titratable.

Data fitting, alternative fittings and confidence intervals

The computationally determined peak heights were used directly in the fit shown in Figure 3. In the figure the signal intensity (au) was normalized to the mole fraction of $Q_B^{\bullet-}$ via the maximum estimate described above. The fit shown in Figure 3 was equally constrained (i.e. the fit parameter [S] was constrained to the estimated max signal).

Under certain conditions ($W_{HH} > 70$ mV, see below), it is possible to arrive at an unambiguous solution without the estimate of the maximal Q_B signal. Figure S3A compares the constrained fit shown in Figure 3 (red) with an unconstrained fit of the same data (blue). The different parameters obtained are summarized in table S1. Whilst the peak position is unaffected, the ΔE of the unconstrained fit is larger by approx. 35 mV. This difference does not impact on any of the conclusions drawn in the paper and is mostly explained by the data analysis method.

In the main paper we used the raw data with minimal normalisation treatment. This might not lead to the best result for the following reasons: firstly, there is a probably a small baseline signal in the $g=2$ region from other organic radicals; secondly, due to some convexity in the background EPR and the way the peak height is determined (finding the minima on both sides of the peak to construct a baseline), especially in the $g = 1.66$ signal, the value doesn't reach zero even though no $g = 1.66$ peak is visible. Thirdly, whilst the signal heights of the $g = 1.66$ and $g = 2$ signals should match in relative terms, there is no physical reason why the absolute signal heights of the two signals should. We used the absolute values without normalisation since they were a coincidentally close match.

To account for these effects a) the baselines can be adjusted and b) the maxima can be adjusted before fitting the data. Figure S3 compares the data and fit used in the main paper (panel A) with a data-set that has been baseline adjusted (panel B) and a dataset that has both the baseline adjustment and the relative intensities of the 1.66 and $g\sim 2$ signals adjusted (panel C). The adjustment of the baseline leads to a better match between the constrained and unconstrained fits, whilst the adjustment of intensities has no observable effect on the quality of the fits. Overall, it was concluded that although the adjusted datasets lead to a better unconstrained fit that is in accordance with the estimated maximum, the added benefit is small and therefore this was left out of the main text to avoid complicating the analysis.

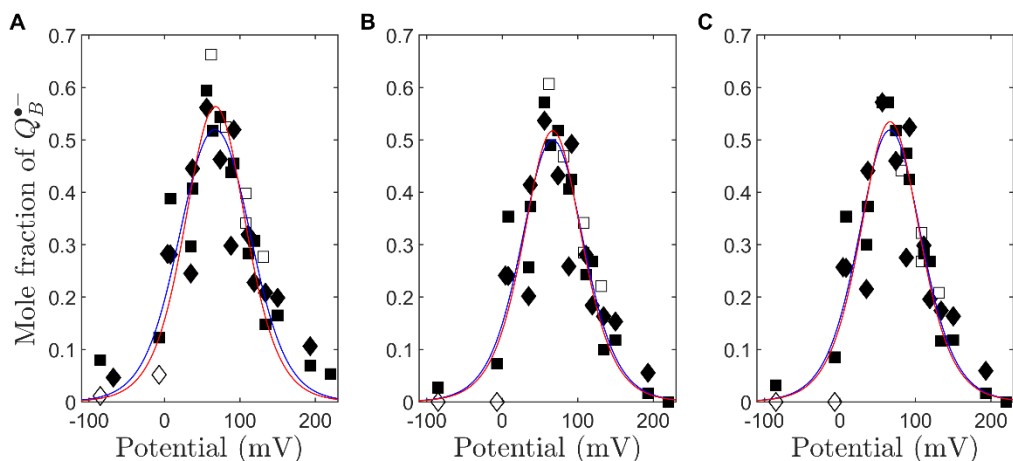


Figure S3 Alternative data treatments and fits. Panel A: Raw data. Panel B: Data adjusted for baseline. Panel C: Data adjusted for baseline and relative intensities. Constrained fits are shown in red and unconstrained fits in blue.

Table S1: Parameters and Confidence intervals for different types of fit and data treatment.

Fit type	E_{\max} (mV) \pm 95% conf int.	ΔE (mV) \pm 95% conf int.
Untreated Data constrained A	67 ± 5	49 ± 37
Untreated Data unconstrained A	67 ± 6	85 ± 30
Baseline adjusted constrained B	67 ± 5	39 ± 40
Baseline adjusted unconstrained B	67 ± 5	54 ± 35
Baseline +intensity adjusted const. C	66 ± 5	38 ± 38
Baseline +intensity adjusted unconst. C	66 ± 5	56 ± 32

The confidence interval in terms of ΔE is an order of magnitude larger than the E_{\max} confidence interval due to the following reason. Even if the raw data is treated, there is noise in the data that is intrinsic to the experimental setup. This leads to uncertainty in both fit parameters. The dependence of ΔE on the width of the bell-curve, however, is not linear. Figure S4 shows the relationship between ΔE and the width of the bell-curve at half height (W_{HH}). At $\Delta E \ll 0$, W_{HH} is independent of ΔE . This means that in this case the shape of the titration curve cannot be used to determine ΔE with confidence and other data (for example the size of [S]) is necessary. In the range $0 \text{ mV} < \Delta E < 100 \text{ mV}$ (as found in the present titration), the dependency is present but weak. That means that small variations in the width of the curve have big effects on the ΔE value (the blue and red curves in Panel B and C are almost identical, whilst the $\Delta \Delta E$ is $\sim 15 \text{ mV}$). Consequently, the observed noise in the data leads to the large 95% confidence intervals in the ΔE value. This also means that without increasing the accuracy of the measurements, simply adding more data-points would not

significantly narrow the confidence intervals. The E_{\max} value does not have the same problem and therefore the confidence interval is smaller.

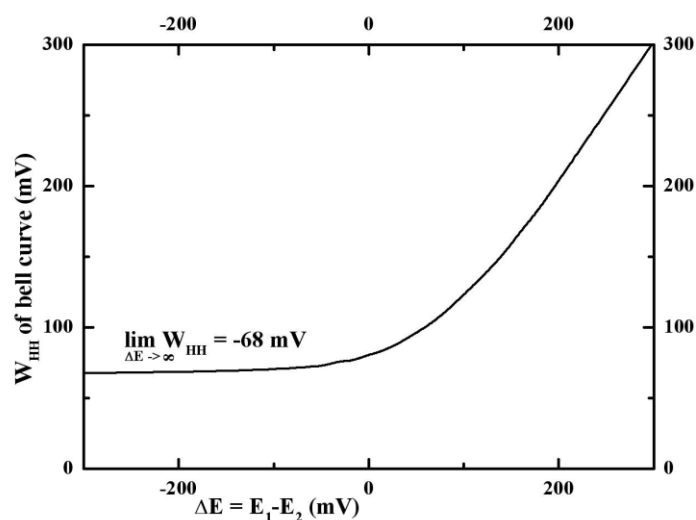


Figure S4: The dependence of the width of the resulting bell-curve (W_{HH}) on the ΔE between the two-electron redox transitions for quinone.

The confidence interval for the midpoint potentials of the two redox couples is determined as follows:

$$\text{Conf.int.}(E_1/E_2) = \text{Conf.int.}(E_{\max}) + \text{Conf.int.}(\Delta E)/2 \quad \text{Eq. S4}$$

In summary, both estimates of ΔE , that from the estimate of the maximum signal and that from the curve fitting, yield very similar results: values of $\Delta E \approx 50$ mV. This suggests that although the EPR titration is noisy and data-points are sparse in the lower potential region, the data-set is sufficient to determine the redox potentials of both couples in a way that supports all our conclusions. Furthermore, this data-set is in good agreement with what is seen in one earlier partial titration on the biradical signal (6) and with several Q_B titrations in the homologous purple bacterial reaction centers (7–9); and they are also consistent with the thermoluminescence derived energy gap (the present work).

Verification of Mn cluster integrity by generation of the S₂ state

The retention of the Mn₄O₅Ca cluster during the course of the titration was assessed in two ways: firstly by the presence of free “hexaquo” Mn²⁺ signals in the spectra, representing the reductive loss of the Mn₄O₅Ca cluster; and secondly, by the ability to form the S₂ multiline signal as a measure of the presence of the normal, stable S₁ of the Mn₄O₅Ca cluster in the dark.

Before adding redox mediators, no free Mn²⁺ was observed. After the addition of redox mediators and equilibration in the dark, a small amount of free Mn²⁺ was detected. This could arise from centres that had lost or displaced one or more of the extrinsic polypeptides at the luminal side of PSII during the purification and were thus more susceptible to reduction. The size of the free Mn²⁺ signals did not increase during the redox titrations. Further evidence that the manganese cluster was retained in most centers was the ability to generate the S₂ multiline signal by illumination at 200 K. Illumination at this temperature has been shown to oxidize the Mn₄O₅Ca cluster from S₁ to S₂ but not to higher S-states (10). This is taken as an indication that the majority of the centres did not lose the Mn₄O₅Ca cluster during the course of the titration and the majority remained in the S₁ state.

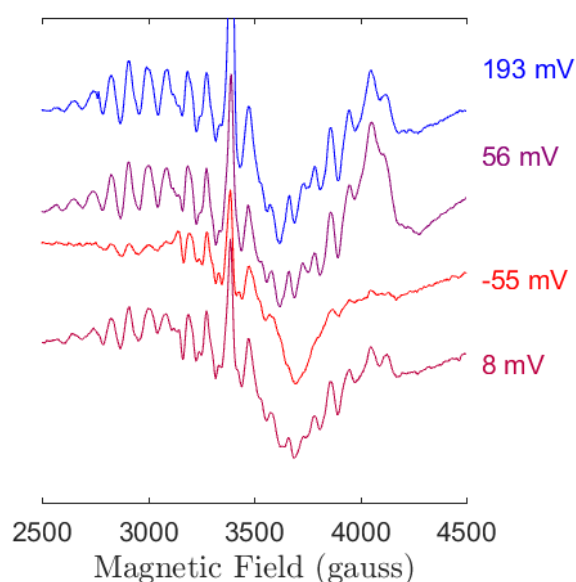


Figure S5: Generation of the S₂ multiline signal by illumination at 200 K. The amplitude of the light induced multiline diminishes in the lowest potential sample but is reformed at higher potentials again. The samples shown from top to bottom were taken successively in the titration, i.e. the 8 mV sample was exposed to all previous potentials.

All samples were first exposed to light at 77 K to generate the $g=1.66$ signal. Thawing at room temperature for 1 minute in darkness was done to allow electron transfer from $Q_A^{\bullet-}$ to Q_B (or to $Q_B^{\bullet-}$) and/or to the oxidised mediators. In the lower-potential samples, however, Q_B is reduced, so $Q_A^{\bullet-}$ oxidation only occurs via the mediators and this may be incomplete at this incubation time. When the samples were re-frozen and illuminated at 200 K, the samples containing PSII in which $Q_A^{\bullet-}$ was still present cannot undergo stable charge separation and therefore do not show the EPR signal from the S_2 state. Any PSII in which the S_1 state was reduced back to S_0 would also be incapable S_2 formation at 200K. Although the intensity of the multiline signal decreased at the lowest potentials, it partially recovered again at higher potentials (see Figure S1). The fact that the recovery is only partial is likely due to a fraction of the centers in the S_1 state being reduced to S_0 at the lowest potentials.

Overall it is clear that the Mn_4O_5Ca -cluster is retained in the majority of centres even after exposure to low potentials.

Calculation of the dissociation constant.

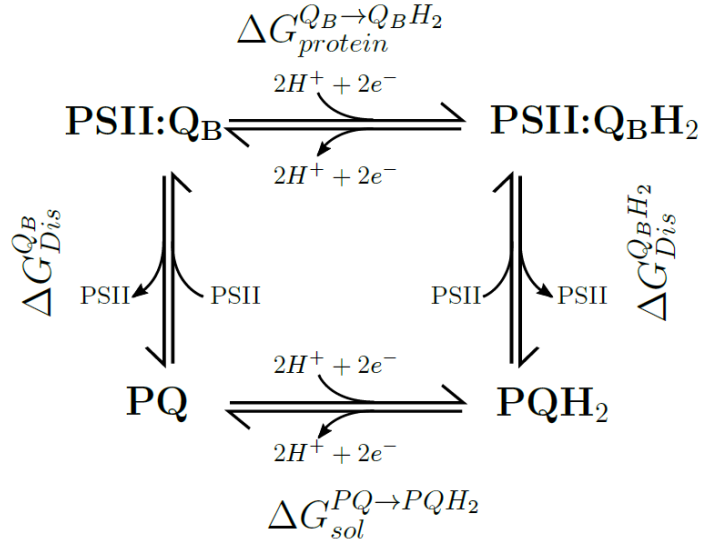


Figure S6: Relationship between the equilibrium dissociation energy (ΔG_{Dis}) and redox energies of the reaction in solution and in the protein.

Figure S6 shows a thermodynamic “box” demonstrating the influence that PQ binding to PSII has on its reduction potential. Both the reduction potentials and the dissociation constants are thermodynamic functions directly related to standard free energy changes (Eq S5 and S6).

$$\Delta G_{dis} = RT \ln(K_{Dis}) \quad \text{Eq. S5}$$

$$\Delta G_{red} = -nF E_{Red} \quad \text{Eq. S6}$$

The free energy change in going from the upper left corner of the “box” to the lower right corner must be identical, being a state function, for the two possible paths. If for example the reduction potential for the free quinone is more positive than when it is bound to PSII, $E_{PQ/PQH_2} > E_{Q_B/Q_B H_2}$, then the reduced quinone, PQH_2 , will have lower affinity for PSII than the oxidised form, PQ, i.e. $K_{Dis}^{Q_B H_2} > K_{Dis}^{Q_B}$. This can be formally described by equation S7:

$$\Delta \Delta G_{protein} = \Delta G_{protein}^{Q_B \rightarrow Q_B H_2} - \Delta G_{sol}^{PQ \rightarrow PQH_2} = \Delta G_{dis}^{Q_B} - \Delta G_{dis}^{Q_B H_2} \quad \text{Eq. S7}$$

Eq. S7 can be rearranged as follows

$$\Delta G_{protein}^{Q_B \rightarrow Q_B H_2} - \Delta G_{sol}^{PQ \rightarrow PQH_2} = RT \ln \left(\frac{K_{Dis}^{Q_B}}{K_{Dis}^{Q_B H_2}} \right) \quad \text{Eq. S7}$$

and the ratio of binding constants calculated:

$$\frac{K_{Dis}^{Q_B}}{K_{Dis}^{Q_B H_2}} = e^{\frac{\Delta G_{protein}^{Q_B \rightarrow Q_B H_2} - \Delta G_{sol}^{PQ \rightarrow PQH_2}}{RT}} \quad \text{Eq. S8}$$

Re-evaluation of literature EPR titrations

EPR-redox titrations present in the literature were digitized from the paper figures (6–9) and re-evaluated using the correct formulae for the concentration of the intermediate semiquinone (see above) .

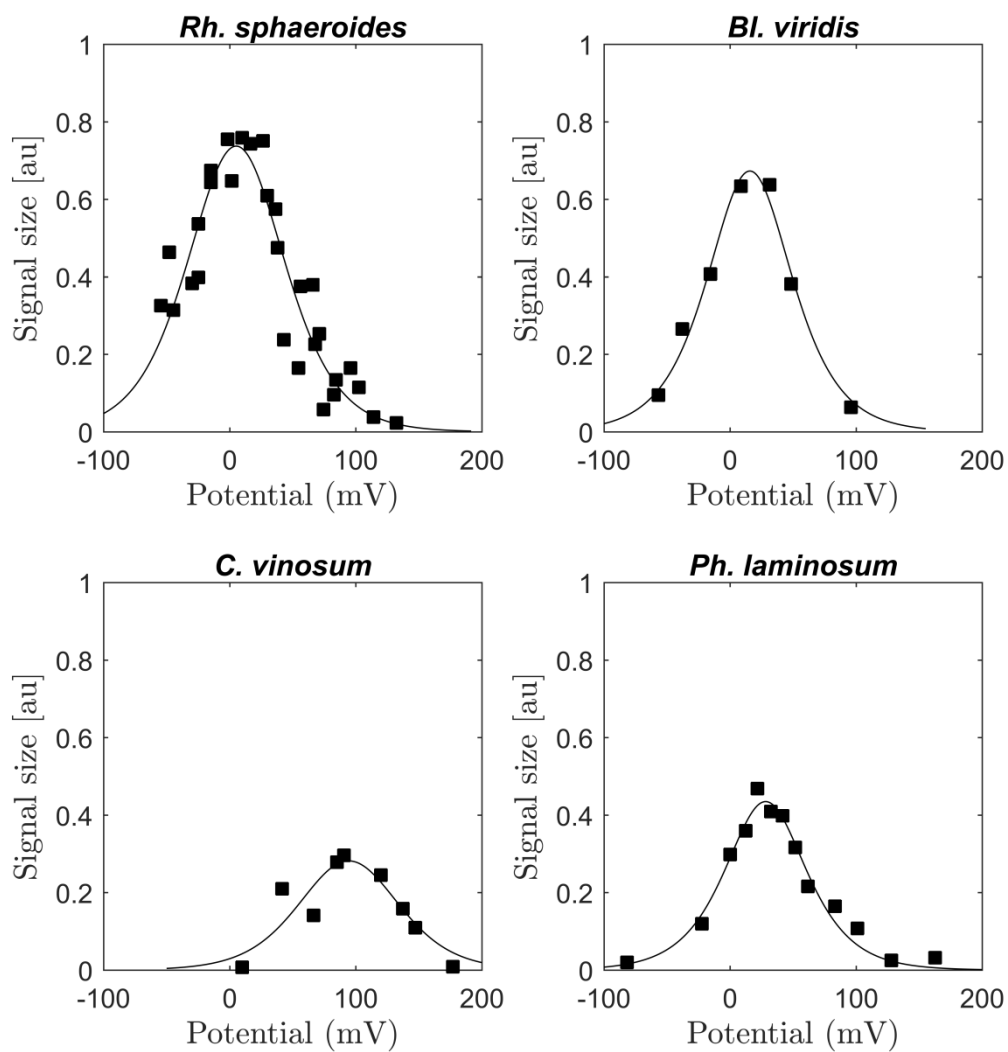


Fig S7: Literature data for titrations of EPR signals arising from $Q_B^{\bullet-}$ (either $Q_B^{\bullet-}Fe^{2+}$ in purple bacteria or from the $Q_A^{\bullet-}Fe^{2+}Q_B^{\bullet-}$ biradical in *Ph.laminosum* PSII) replotted and reanalysed. Data digitized from (6–9).

Table S2. Values derived from fitting literature titrations.

Organism	E_{max} (peak pos.) [mV]	ΔE [mV]	% of total Q_B [%]	E_{max} @ pH7 (E_1, E_2) [mV]
<i>Rh. sphaeroides</i> pH 8	5 ± 9	36 ± 41	76	64 (82, 46)
<i>Bl. viridis</i> pH 8	16 ± 11	-5 ± 89	29	75 (72.5, 77.5)
<i>C. vinosum</i> pH 7	94 ± 31	45 ± 115	58	94 (116.5, 71.5)
<i>Ph. laminosum</i> pH 8	28 ± 8	-21 ± 82	27	86 (75.5, 96.5)

For Q_B in purple bacteria the E_m values (E_1 and E_2 in table S2) are slightly different from those in the original publications in which the data were fitted as separate non-interacting $n=1$ curves. The present values can be taken as improvements compared to the originals but they still suffer from significant uncertainties arising from the lack of an independent estimate of the maximum size of the signals. Nevertheless, in all three cases it is clear that the semiquinone is thermodynamically stabilised, as found in here for PSII, however the degree of stabilisation seems to show some variation. All of the purple bacteria have ubiquinone as the membrane quinone pool and thus as Q_B . The E_m of pool UQ/UQH₂ is 90mV, 20-30mV lower than that for PQ (37). For *Rh. sphaeroides*, the best studied species, the average E_m for the two couples is 64mV, which is 26 meV more reducing than the value of the pool. Following the interpretation giving for PSII in the main text, this difference represents the driving force for $Q_B H_2$ release, and corresponds to a preferential binding of UQ over UQH₂. This effect is smaller than in PSII but is qualitatively consistent with estimates from computational studies (38). The average value for the two quinone redox couples for *Bl. viridis* indicates less driving force, while that for *C. vinosum* seems to indicate no driving force, a situation which is commonly assumed to be the case (e.g. 15-17). These variations, if significant, could reflect the difference functional redox environments (low O₂ vs high O₂ in PSII) and different functional roles (the purple bacterial reaction center driving a cyclic electron transfer chain vs a PSII at the start of a linear electron transfer chain).

The current work clarifies our bioenergetics understanding of Q_B function in Type 2 reaction centers, it also helps complete our understanding of the quinone binding sites in photosynthesis. A reviewer requested a comparison the bioenergetics of quinones in photosynthetic reaction centres.

Pool quinones function as $n = 2$ electron carriers, where the ΔE between the two redox couples is strongly negative (~ -500 mV) reflecting a highly unstable semiquinone that is both a strong reductant and a strong oxidant. The first reduction step ($Q/Q^{\bullet-}$) is much more difficult and thus occurs at a lower potential, due to the relatively apolar membrane environment. In contrast the second reduction step, $Q^{\bullet-}/QH_2$, occurs very easily, thus with high potential E_m because the reduction is facilitated by the easy access of the charged semiquinone state to the protons at the interface of the membrane and the aqueous phase.

Q_B has ΔE values at close to 0 meV or slightly positive (0 to +50meV). This reflects the higher potential E_m for the 1-electron Q_B/Q_B^- couple compared to that in the pool. This higher potential is due to the positive charges on the non-heme Fe^{2+} (39), the H-bonds to the carbonyls and the proton uptake at D1-His252 to Q_B that is associated with the distal H-bonding D1-Ser264 (31). The reduction semiquinone to form the hydroquinone, $Q_B^{\cdot-}/Q_BH_2$ is made more difficult in the Q_B site compared to the equivalent redox step in the pool by restricting the protonation events: the protonation that occurs upon $Q_B^{\cdot-}$ formation is on the adjacent amino-acid but not on the semiquinone itself. The protonation of $Q_B^{\cdot-}$ itself only occurs on the second turnover and is thought to be triggered when $Q_A^{\cdot-}$ is generated (31).

Q_A functions as 1-electron relay as the Q_A/Q_A^- couple. Its modestly low E_m , around -150 mV, is attributed to charge compensation by the non-heme Fe^{2+} and by the H-bonds from amino acids to the quinone carbonyls (39), but it is lower than that for Q_B because the charge on $Q_A^{\cdot-}$ is not compensated by proton uptake, nor by the proximity of more polar groups (31). This reflects the Q_A site, which is relatively apolar, lacks ionisable groups and from which water is excluded. This results in the second reduction step being exceptionally difficult, with a $\Delta E > \sim +300\text{meV}$, i.e. a greatly stabilised semiquinone that only acts as 1-electron relay. The theoretical E_m for the second reduction of $Q_A^{\cdot-}$ presumably occurs at a potential so low that it is irrelevant for normal function. Persistent over-reduction, chemically or by photo-driven Pheo $^{\cdot-}$ formation in the presence of $Q_A^{\cdot-}$, results in the second reduction step which is presumably accompanied by protonation due to modification of the native site (40).

The A_1 phylloquinones in PSI play a 1-electron relay function like that of Q_A but with a much lower E_m due to the absence of the Fe^{2+} and presence instead of the negatively charged F_X cluster (39). Protonation of $A_1^{\cdot-}$ seems unlikely given, i) the rapid rate of forward electron transfer, ii) the crystal structure, and ii) their location (further from the aqueous medium compared to the Type 2 quinones). Protonation reactions associated with a nearby amino acid associated with structured waters in the vicinity of A_{1A} have been suggested to occur in high light based on computational studies (41). Similar over-reduction driven by strong light seem to lead to double reduction as first seen in Type 2 reaction centres. Overall it seems that the PSI A_1 phylloquinones are similar to Q_A in so far as their second reduction potential is lower than the 1-electron couple. Thus we might predict a ΔE between the two redox couples that is strongly positive, $\sim +200\text{meV}$ or more, giving a “stabilised” semiquinone, despite its reductive reactivity as a 1-electron donor.

Thermoluminescence experiments

Data analysis: To determine the peak positions of the TL curves, the data was smoothed with a gaussian filter ($\sigma = 5.8$ s) before finding the local maxima computationally with Matlab.

Multiple TL bands are present in our experiments. When the bands are too close together the peak temperatures of individual bands cannot be reliably deconvoluted without some kind of model-based fitting. The current TL model (11) is not quantitative and is thus not reliable (e.g. (12)).

The peak temperature of the TL band can be determined with enough accuracy when a single band is present, when one band dominates or when the separation between the peak temperatures is large. This seems to be the case in our experiments when the dominant peak represents the $S_2Q_B^{\bullet-}$ recombination within the pH range of 6.5 -7.8 (See Fig. S12 and S13). At lower pH values the C-band is present and shifts the peak temperature higher, whilst at high pH values other bands are present, e.g. $S_2Q_BH_2$ recombination (see the discussion section on the stabilisation of the semiquinone within the Q_B site) that contribute to lower temperature luminescence. To avoid those complications only the values in the pH range between 6.5 and 7.8 were used for the calculations

Additional dataset: the original dataset used in the paper was based on the average of two TL curves (Figures S8 and S10), in response to a reviewer's comments, we repeated the experiment, (with the slightly different pH values), and got essentially the same result (Figures S9 and S11). There is some difference in the peak temperature and intensity of the DCMU-induced $S_2Q_A^{\bullet-}$ recombination, which may be attributed to small differences in the material or experimental conditions (See Fig S13). This difference results in an increase in the energy gap between $Q_A/Q_A^{\bullet-}$ and $Q_B/Q_B^{\bullet-}$ of around 20 meV. The energy gap between Q_A to $Q_B^{\bullet-}$ energy gap is estimated to be 180-200 meV.

While our estimates of the peak position may have some inaccuracy, especially at high and low pH, the data themselves are very similar to those of Vass and Inoue (13). A similar treatment applied to their data gives a gap value of 210 meV. The presence of DCMU is expected to up-shift the potential of $E_m(Q_A/Q_A^{\bullet-})$ by 50meV. This would increase the energy gap accordingly. While there are no direct measurements of the DCMU effect on *T. elongatus* cores, the temperature difference for the TL peak position for $S_2Q_A^{\bullet-}$ recombination with DCMU vs that with bromoxynil were found to be similar to those in plant PSII (14), indicating a similar effect of DCMU in *T. elongatus* and plant PSII. Whether or not we apply a DCMU adjustment, the experimental data indicate a gap between Q_A and Q_B of ~200 mV,

significantly bigger than the ~ 80 meV, as previously derived from thermoluminescence and kinetic measurements (11, 15).

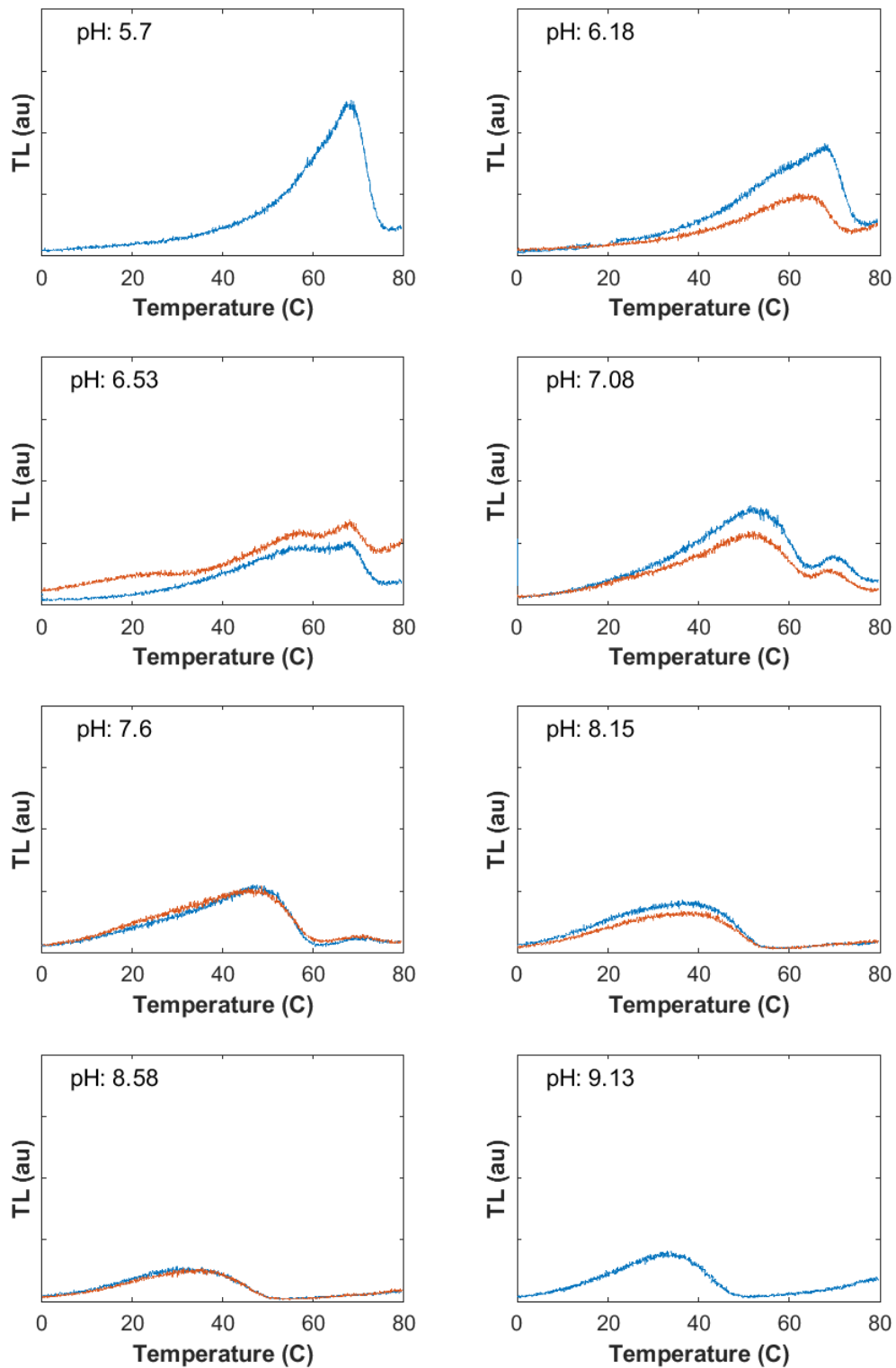


Figure S8: pH dependence of TL after one flash in *T. elongatus* PSII cores. Scan rate 0.33 $^{\circ}\text{C s}^{-1}$; Dataset 1.

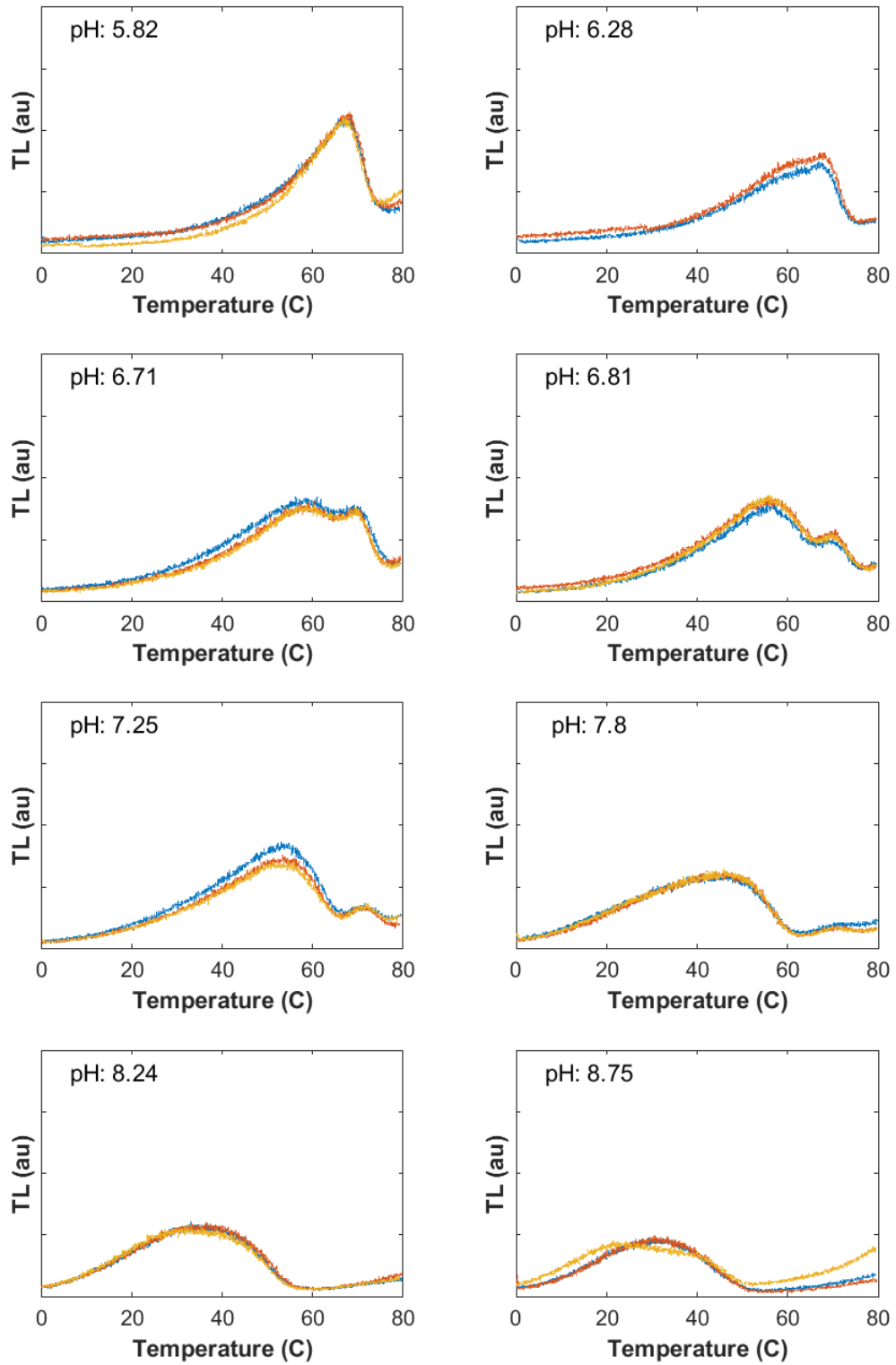


Figure S9: pH dependence of TL after one flash in *T. elongatus* PSII cores. Scan rate $0.33\text{ }^{\circ}\text{C s}^{-1}$; Dataset 2.

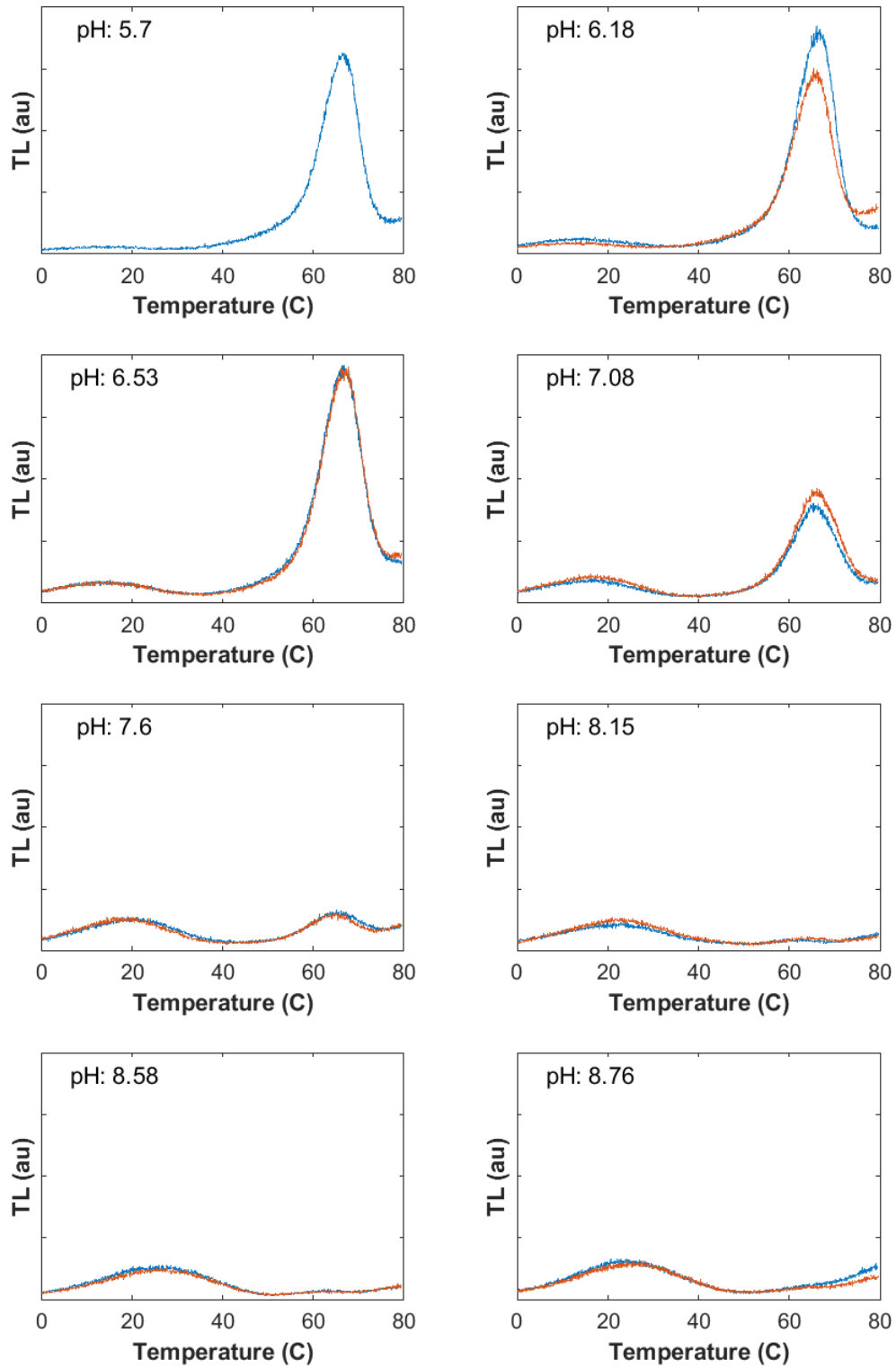


Figure S10: pH dependence of TL after one flash in *T. elongatus* PSII cores in the presence of 10 mM DCMU. Scan rate: $0.33\text{ }^{\circ}\text{C s}^{-1}$; Dataset 1.

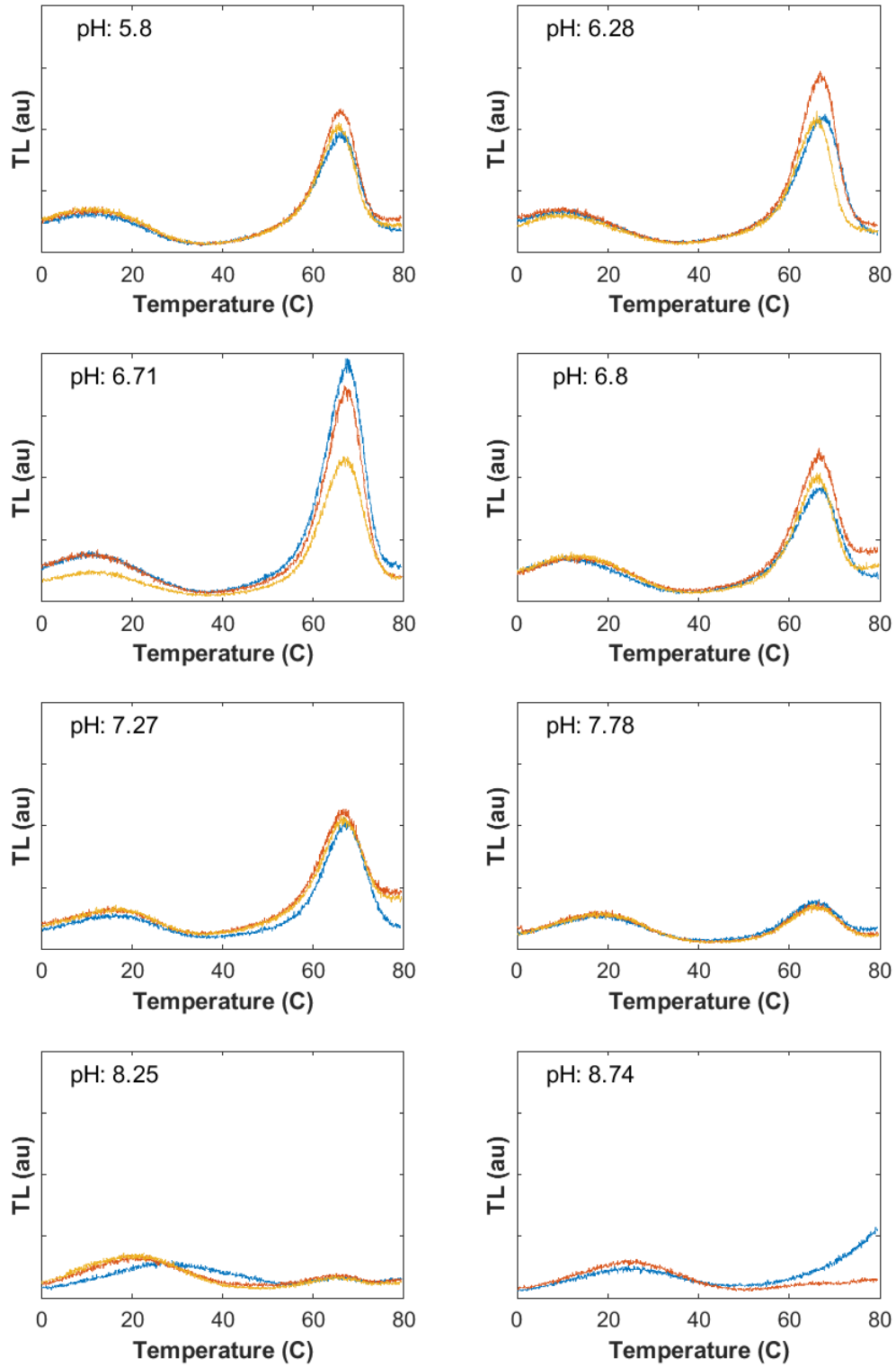


Figure S11: pH dependence of TL after one flash in *T. elongatus* PSII cores in the presence of 10 mM DCMU. Scan rate: $0.33\text{ }^{\circ}\text{C s}^{-1}$; Dataset 2.

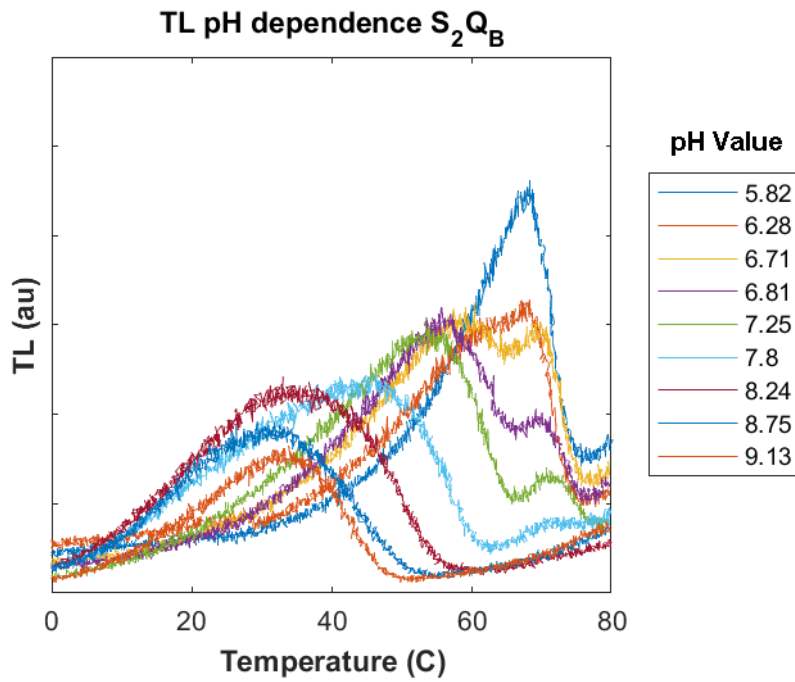


Figure S12: Example of the effect of pH on the TL curves from *T. elongatus* PSII cores. This plot represents one of the three pH data sets that constituted data set 2.

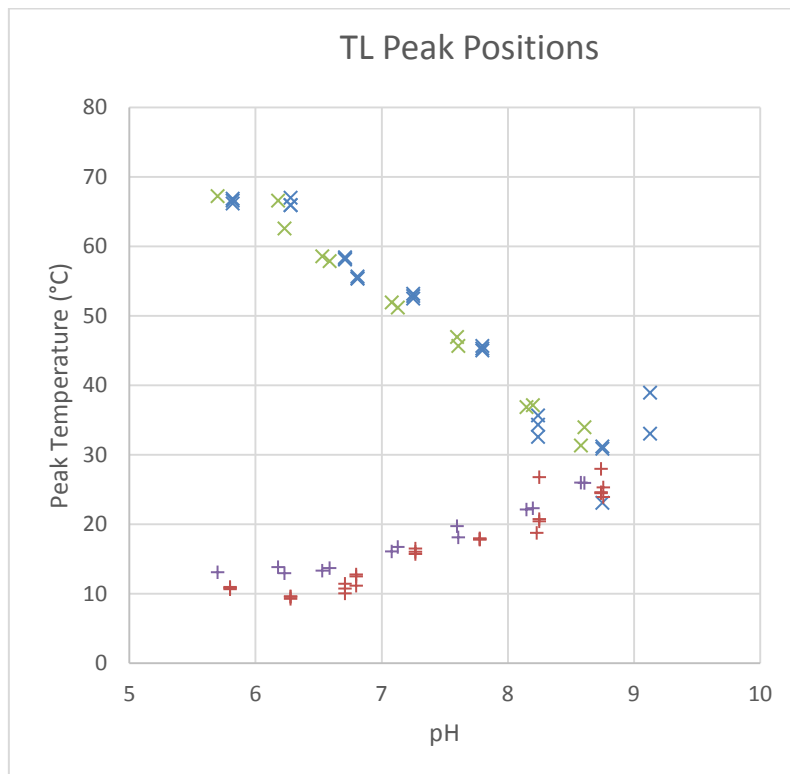


Figure S13. Comparison of the pH dependence of the TL peak temperatures from Data sets 1 and 2, with and without DCMU. Green X: Dataset 1; Blue X: Dataset 2; Purple +: Data set 1 + DCMU; Red +: Data set 2 + DCMU.

The difference in redox potentials between Q_A and Q_B

The difference in redox potentials between the $Q_A/Q_A^{\bullet-}$ and $Q_B/Q_B^{\bullet-}$ couples reported here ~ 180 meV (or ~ 230 meV if there is a DCMU effect) is larger than previously estimated (70 – 80 meV) (11, 16). Here we discuss possible origins of this discrepancy. We shall cover specific characteristics of the methods used and the estimates of the relevant redox potentials, that of Q_A from the literature and that of Q_B from the present work.

The earlier estimates of the energy gap between Q_A and Q_B were based on estimates of the equilibrium constant that were obtained from the kinetics of the forward and backward electron transfer reactions between Q_A and Q_B in a range of dynamic states (16–21), while the dark equilibrium potentiometric method used here requires equilibration over a long period, in which short-lived states decay, protons move and relaxations occur. While the two methods used for the estimates reflect different situations, the equilibrium redox titration method would seem appropriate for Q_B given the stability of its redox states. For Q_A , the forward electron transfer takes place in the sub millisecond-millisecond time-scale and thus may be different when formed via a back-reaction or under equilibrium titration conditions.

The mismatch of the two estimates for the $Q_A/Q_A^{\bullet-}$ to $Q_B/Q_B^{\bullet-}$ energy gap may also be partially attributed to the fact that the “gating effect”, rather than the driving force, determines the rate-limiting step for the $Q_A^{\bullet-}$ to Q_B reaction in the purple bacterial reaction centers (22). The chemical nature of the gating process remains uncertain but is generally attributed to small-scale protein and/or cofactor movements associated with the proton-coupled electron transfer (23–25). In PSII several reports indicate a similar situation exists (26–28) and similar gating is assumed to be present (26–31). This gating effect is not included in the treatments used to deduce the equilibrium constant and could therefore contribute to the mismatch in the estimates of the $Q_A/Q_A^{\bullet-}$ to $Q_B/Q_B^{\bullet-}$ energy gap from kinetic measurements.

Another difference between the kinetic and the equilibrium methods is that kinetic methods are done in the presence of an oxidised electron donor-side component (usually S_2), while the equilibrium method is done in the dark S_1 state (see below). This may be a non-innocent difference because the donor-side can affect the redox behaviour of the electron acceptors in PSII (30).

The E_m of $Q_A/Q_A^{\bullet-}$ obtained from redox titrations is susceptible to being underestimated, i.e. found to be more negative than in functional conditions. An intrinsic property of redox titrations of multi-cofactor proteins is that the titration of lower potential components must be done in the presence of the reduced form of the, often adjacent, higher potential components. This can result in a shift in the potential of the lower potential component(s) compared to functional conditions. In this case, Q_B is the highest potential component in the complex, so it will not be influenced by any higher potential components. In contrast, Q_A will inevitably be titrated in the presence of Q_BH_2 , whilst in functional conditions $Q_A^{\bullet-}$ is formed with the oxidised form, Q_B , present. To explain the difference between the energy gaps based on kinetic measurements compared to those based on equilibrium redox titrations, the binding of Q_BH_2 would have to shift the E_m of $Q_A/Q_A^{\bullet-}$ by ~ -150 mV. It is known that binding of herbicides in the Q_B site can shift the $E_m(Q_A/Q_A^{\bullet-})$ by ~ 50 mV, either positive or negative depending on the herbicide (32). While an effect of Q_BH_2 binding on the E_m of $Q_A/Q_A^{\bullet-}$ could contribute to the discrepancy such a big effect would be unexpected although not impossible.

Another complicating factor is the effect of the electron donor-side components on the redox properties of the electron acceptors. If the Mn_4CaO_5 cluster were lost during the titration, it would have changed the E_m $Q_A/Q_A^{\bullet-}$ (33) and potentially perturb the Q_B^- redox properties. Thus we monitored the cluster and found it remained intact in the vast majority of centers during the course of the titrations. Nevertheless, the redox state of the cluster may have changed from S_1 to a lower S-state in a small fraction of the centres at the lowest potentials used (see above). This could contribute in some way to the scatter in the data at lower potentials in titrations reported here. However, given the low potentials needed and the low proportion of centres in which it occurs, it would have had little influence of the measured potentials of Q_B/Q_B^- couple. S-state reduction is more likely to occur in the Q_A titrations as lower potentials are needed, thus a putative Mn-cluster reduction effect would be expected to affect the Q_A E_m value more than the Q_B E_m values.

Discussion of the Kato *et al* 2016 paper

Our findings conflict with recent work by Kato *et al.* (3). In the following we briefly explain their method, the potential flaws and how their results can be rationalized in light of our present findings.

Background: Method used by Kato *et al.*

To determine the redox potentials of a two-electron redox transition one needs to determine the concentration of either the oxidized or the intermediate or the reduced species as a function of the applied potential. Kato *et al* (3) used spectroelectrochemistry and light-induced FTIR difference spectroscopy to determine the potential of Q_B in PSII. Neither of the three principal species ($[Q_B]/[Q_B^{\bullet-}]/[Q_BH_2]$) is measurable directly with FTIR. What is measured instead, is the ability to form a difference signal related to $Q_B^{\bullet-}$ upon flash illumination (a CO stretching vibration of a nearby Pheophytin) termed α .

$$\alpha = ([Q_B] - [Q_B^{\bullet-}])/[Q_B]_0$$

$$[Q_B]_0 = ([Q_B] + [Q_B^{\bullet-}] + [Q_BH_2])$$

When the quinone in the Q_B site is fully oxidized, the flash generates $Q_B^{\bullet-}$ and the maximal signal is seen in the difference spectrum. When the quinone in the Q_B site is fully reduced, i.e. Q_BH_2 is present, the flash cannot generate any $Q_B^{\bullet-}$ and therefore no signal can be seen in the difference spectrum. What happens in between those two extremes depends on the ΔE between the two couples $Q_B/Q_B^{\bullet-}$ and $Q_B^{\bullet-}/Q_BH_2$ and is reproduced below in the supplementary Figure Kato *et al* S4 (3).

If the ΔE (the energy gap between the two redox couples) is very large, i.e. the $Q_B^{\bullet-}$ is strongly stabilized, a dependence of the difference signal on the applied potential as shown in blue in Figure Kato *et al* S4 would be expected. As the potential is lowered (going from right to left in Fig Kato *et al* S4), the observed difference signal decreases, because more $Q_B^{\bullet-}$ is already present in the dark spectrum prior to the flash. When the $Q_B/Q_B^{\bullet-}$ ratio is 1, i.e. the applied potential equals the $E_m(Q_B/Q_B^{\bullet-})$, no signal can be observed because equal amounts of $Q_B^{\bullet-}$ are generated and removed by reduction to Q_BH_2 . When the potential is further reduced to the point where 100 % $Q_B^{\bullet-}$ is present in the dark, a subsequent flash will turn over all the centers to the Q_BH_2 state and therefore the difference signal will be maximally

negative. At even lower potentials $Q_B H_2$ is formed in the dark and light-induced changes associated with Q_B function are lost.

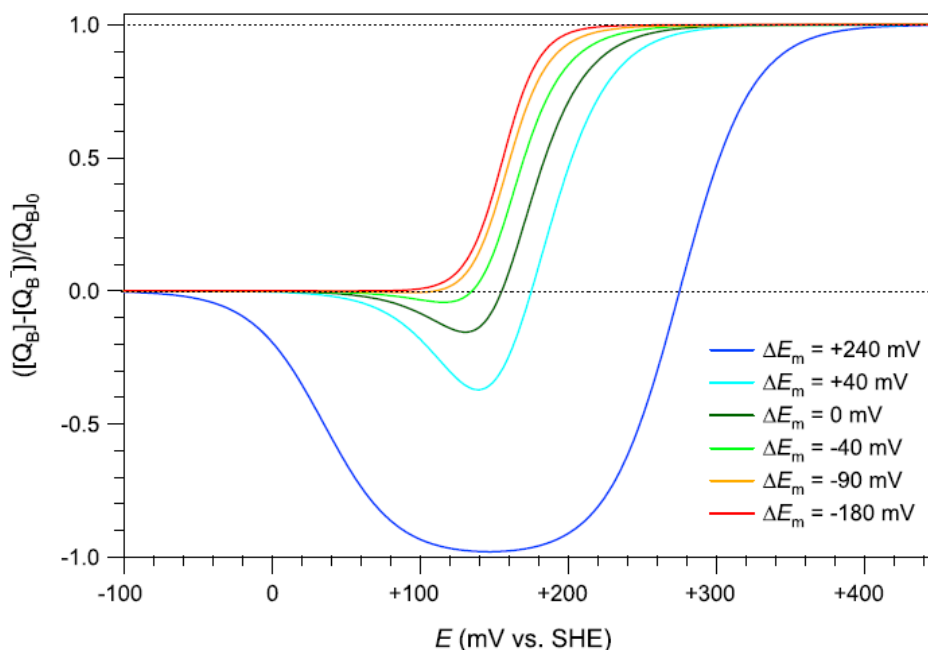


Fig. Kato *et al* S4. Simulated Nernst curves for the mole fraction difference between Q_B and Q_B^- ($[Q_B]/[Q_B]_0 - [Q_B^-]/[Q_B^-]_0$) against electrode potential E at $10\text{ }^\circ\text{C}$ for various $\Delta E_m (= E_m^1 - E_m^2)$. $\Delta E_m = +240\text{ mV}$ (blue lines; $E_m^1 = +275\text{ mV}$, $E_m^2 = +35\text{ mV}$), $+40\text{ mV}$ (light blue lines; $E_m^1 = +175\text{ mV}$, $E_m^2 = +135\text{ mV}$), 0 mV (green lines; $E_m^1 = E_m^2 = +155\text{ mV}$), -40 mV (light green lines; $E_m^1 = +135\text{ mV}$, $E_m^2 = +175\text{ mV}$), -90 mV (brown lines; $E_m^1 = +110\text{ mV}$, $E_m^2 = +200\text{ mV}$), -180 mV (red lines; $E_m^1 = +65\text{ mV}$, $E_m^2 = +245\text{ mV}$). Reprinted from ref. 3 .

If ΔE is significantly negative no thermodynamically stable intermediate $Q_B^{\bullet-}$ is formed prior to the flash. Instead Q_B would undergo a two-electron, two-proton reaction to form $Q_B H_2$ directly with an $n = 2$ Nernst relationship. As the ability to form the difference signal α in this case depends solely on the concentration of Q_B in the dark, α also shows an $n = 2$ Nernst behaviour with regard to the applied potential. This is exemplified by the red curve in Fig Kato *et al* S4 ($\Delta E = -180\text{ mV}$).

This method can in principle be used to monitor the redox potential of $Q_B^{\bullet-}$, however the paper of Kato *et al* (3) appears to have three fundamental flaws that might each individually compromise the results and conclusions. We will discuss these in detail in the following.

1 Potential problem related to the indirect nature of FTIR measurements.

The FTIR probe for $Q_B^{\bullet-}$ used by Kato *et al* is not a direct measurement of any of the involved species ($Q_B/Q_B^{\bullet-}/Q_BH_2$). There is a crucial difference between measuring the concentration of $Q_B^{\bullet-}$ present in the dark due to the redox equilibrium and the ability to generate $Q_B^{\bullet-}$ with a flash. To obtain the latter, differences of six individual spectra were required for each datapoint (shown in Fig. S14). The ability to detect a temporary formation of $Q_B^{\bullet-}$ by FTIR depends on more factors than just the presence of oxidized quinone and this introduces a variety of possible sources of error.

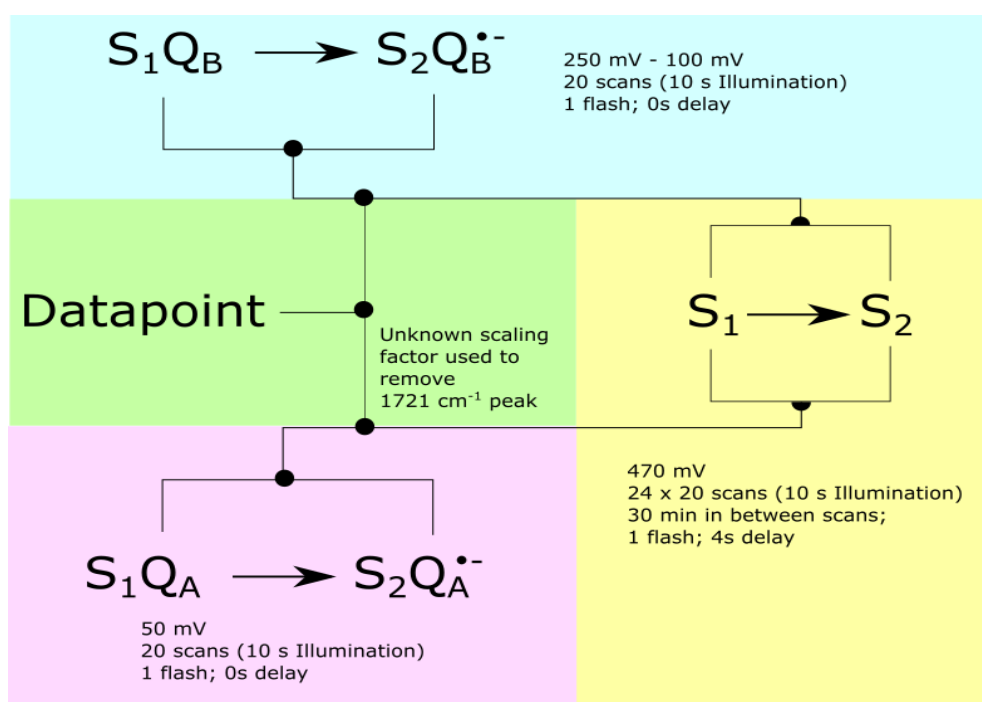


Fig. S14 FTIR protocol to generate the spectra in Fig Kato *et al* 4A. Each black dot represents a difference spectrum.

- i) Is the flash-induced $Q_B^{\bullet-}$ signal stable during the accumulation of the various required spectra? The flash-induced data took at least 10 seconds to accumulate (20 x 10s scans). In that time it is crucial that the reduced forms of Q_B are not reoxidized by the mediators and this must be the case over the whole titration range. The materials and methods however indicate that the $Q_B^{\bullet-}$ lifetime is in the order of the scan time: it is stated that “In the case of the S_2/S_1 difference spectrum, a 4s delay was inserted after flash illumination to reduce the contamination of the $Q_B/Q_B^{\bullet-}$ signals.” Thus a 4 s delay at 470 mV is enough to reoxidize $Q_B^{\bullet-}$ completely, whilst in the range of the titration (100 to 250 mV)

$Q_B^{\bullet-}$ is stable during the 10 s scans and not reoxidized by the mediators. Given the change in the concentration of the active mediator in this range, different reoxidation rates may be expected as a function of potential.

- ii) Similarly, the method of subtracting the S_2/S_1 spectrum taken at 470 mV to generate a pure $Q_B/Q_B^{\bullet-}$ spectrum could run into problems during the course of the titration, as it relies on there being no background spectral changes over the course of the titration. The reduced mediators might donate to the S_2 formed on the flash during the time needed to take the data (at least 20 scans at 10s per scan) and this will change during the course of the titration. It also seems possible that the difference spectra could be perturbed by the reduction of other PSII redox components during the course of the titration (i.e. Tyr_D^{\bullet} , Cyt b559, Cyt c550, even S_1) and any of these could potentially cause problems with the systematic subtraction of the pure S_2/S_1 difference spectrum.
- iii) A light-minus-dark spectrum taken at 50 mV was subtracted from the spectra at all higher potentials. This was done to eliminate the overlapping $Q_A^{\bullet-}$ contribution to the 1745 cm^{-1} $Q_B^{\bullet-}$ peak. This spectrum however, was scaled differently each time (on the basis of the peak intensity of the adjacent non-overlapping 1721 cm^{-1} peak from $Q_A^{\bullet-}$). The scaling factor used for each potential was not given in the paper nor the SI and in the final spectra shown (Fig 3A in Kato *et al*) the 1721 peak remains present at a range of potentials casting some doubt on the spectral manipulations needed to obtain the final data.

In passing, a plot of the 1721 peak from $Q_A^{\bullet-}$ formed upon a flash as a function of potential should give a titration of the redox state of Q_B . This plot in some ways would be preferable to the plot of the light-induced $Q_B^{\bullet-}$ as it does not require the additional subtraction step.

A second point in passing: the 50 mV point at pH6.5 (equivalent to 79 mV at pH 7 in the present work) is within the zone where $Q_B^{\bullet-}$ is thermodynamically stable in a fraction of the centres. Should any $Q_B^{\bullet-}$ have been formed in the titration of Kato *et al*, say through longer incubation time with the limited mediation used, then this would have given a light-induced negative signal, due to the disappearance of

$Q_B^{\bullet-}$. The subsequent subtraction of this from the experiment spectra could have effectively removed the key indicator of the presence of thermodynamically stable $Q_B^{\bullet-}$ from the data in this crucial redox range.

Conclusion. It can be seen that the FTIR redox titration is a very complicated measurement, requiring 6 weighted subtractions, which increase the uncertainty of the experimental data. It seems clear that the claim made in the abstract of Kato *et al* (3) “the E_m value of Q_B reduction was measured directly” is not justified.

2) Potential problems with the redox titration itself

It is well demonstrated that *T. elongatus* cores are isolated with 1 to 2 PQ molecules in addition to Q_A and Q_B and that these function as a “mini-PQ pool” (28, 34, 35). We also know that the PQ pool is reported to have an E_m at 117 mV and to function as an $n = 2$ couple (36, 37).

In a titration starting at a potential where all the quinones are oxidized and titrating in a reducing direction, the PQ pool becomes reduced (PQH_2) before the quinone in the Q_B site. As quinone exchange processes happen on the ms timescale (whilst titrations go for hours), PQH_2 would then exchange with the quinone in the Q_B site (i.e. Q_B) forming Q_BH_2 . The quinone released into the pool would be easily reduced to PQH_2 by the mediators so that all quinones, within the Q_B site and in the pool, would be reduced. In principle, with adequate mediation, the Q_BH_2 in the site should be reoxidized by the mediators, returning it to the Q_B state (or the $Q_B^{\bullet-}$ state depending on the potential). If, however the mediators were too slow, or ineffective in reoxidizing Q_BH_2 , then the ability to form Q_B or $Q_B^{\bullet-}$ would be lost and the quinone within the Q_B site would follow the redox behaviour of the pool. Under these conditions one would observe an $n = 2$ Nernst dependency at the potential of the pool even though the detection method is specifically measuring the redox state of Q_B in the site. Only one mediator is present at potentials where the PQ pool undergoes reduction (hydroxyl-PMS predicted $E_{m_{6.5}}$ of 78mV) and it appears to have been chosen to allow $Q_B^{\bullet-}$ to be stable for at least 10s (see section on FTIR). It thus seems reasonable to suggest that the QH_2 present in the Q_B site is poorly mediated and this gives rise to the loss of flash-induced Q_B reduction tracking with the redox properties of the free quinone pool. This situation would completely explain the contradiction between the two sets of results.

The slight shift in their measured value (125 mV when adjusted to pH7) from the literature value (117 mV) for the pool quinone, if significant, might be attributed to the environment of the free PQ within the cavities, lipids and detergent of the isolated PSII core complex, which could be slightly different to that of PQ in the lipid membrane.

In passing we also remark that Kato *et al* (3) had only 7 points in the plots and crucially have no points at potentials lower than 120 mV. Thus they avoid the region where most of the Q_B redox changes occur. Thus the titration is incomplete. Also Kato *et al* do not appear to have any points taken in the oxidizing direction.

3) Potential problems with data analysis

Regardless of the potential technical problems discussed in the previous sections, here we deal with specific problems with the data analysis done in Kato *et al* (3) which directly concern the validity of the conclusions made.

The fitting procedures used provided the energy difference between the two 1-electron couples of Q_B and a value for ΔE of -120 mV was obtained. In Fig Kato *et al* S4, shown above, this lies between the red and orange curves. From that graph alone, it is obvious that the fittings are not justified as they are barely distinguishable and if the red and orange curves had been centred around their midpoints, this would be even more obvious. This is due to the nature of two-electron transitions.

Experimentally, a determination of the ΔE from the potential dependence of either $[Q_B]$ or $[Q_BH_2]$ is only possible in the zone in which the ΔE is between -50 mV and +50 mV. Only in this region do the slopes of observed Nernst curves diverge enough from the ideal $n = 1$ and $n = 2$ curves to allow the ΔE to be determined. Figure S15 illustrates how a titration curve of either the fully reduced or fully oxidized species relates to the $n = 1$ and $n = 2$ extremes in the zone where ΔE is between -50 mV and +50 mV.

What was actually titrated by Kato *et al* (3) was $\alpha \left(\frac{[Q_B] - [Q_B^{\bullet-}]}{[Q_B]_{total}} \right)$ and therefore the upper boundary of ΔE (+50 mV) does not apply. The lower boundary, however, should remain more or less the same because the influence of $Q_B^{\bullet-}$ decreases at low ΔE values. If one fits a curve to a dataset that is too close to an $n=1$ or $n=2$ curve, any values produced by the fitting algorithm are determined by the boundary conditions of the algorithm and not the actual data. We suggest that this is the case in the work of Kato *et al* (3) and the only valid

conclusions that could have been drawn from their data are that the $E_m(Q_B/Q_B^{\bullet-}) < 130$ mV and that the $E_m(Q_B/Q_BH_2) > 190$ mV. In other words, what is measured is an $n = 2$ transition typical of a “pool” quinone. This is visible in Fig 3C of Kato *et al*, in which the $n = 2$ lines (dotted) seem to be an equally good fit to the data as the simulated curves.

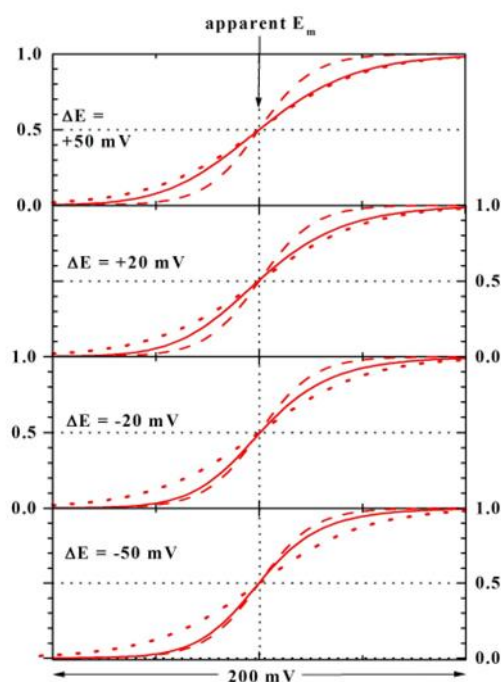


Fig. S15 Hypothetical titration curves (solid lines) of an oxidized species in a 2-electron redox transitions for the region in which ΔE is between -50 mV and +50mV compared to an $n=2$ curves (dashed lines) and an $n=1$ curve (dotted lines).

Conclusions

There are serious doubts concerning the method and the data analysis in Kato *et al* (3). There are several other reasons to doubt their results. 1) It is not what is seen in the literature in the homologous system in bacterial reaction centre (7–9). 2) The redox potential for the two Q_B redox couples reported by Kato *et al* (3), which are indistinguishable from an $n=2$ transition, are difficult to rationalise biologically (see main text). In their results there is no driving force for the release of the product (PQH_2), indeed a small amount of energy would be required, and the Q_B binding site would have a small preference for binding the product (PQH_2) over the substrate: these are properties that would disfavour photosynthetic electron transfer.

Finally, the experimental observations made in the present work, demonstrate that the Kato *et al* (3) findings cannot be correct. We have unambiguously shown the formation of $Q_B^{\bullet-}$ by means of direct EPR measurements of the $Q_B^{\bullet-}Fe^{2+}$ signals in equilibrium titrations. This $Q_B^{\bullet-}$ is formed in the dark and is thermodynamically stable. A thermodynamically stable semiquinone is simply not possible in the context of the Kato *et al* result (i.e. if the $Q_B^{\bullet-}/Q_BH_2$ couple was 120 mV more oxidizing than the $Q_B/Q_B^{\bullet-}$ couple).

References

1. Mühlenhoff U, Chauvat F (1996) Gene transfer and manipulation in the thermophilic cyanobacterium *Synechococcus elongatus*. *Mol Gen Genet MGG* 252(1–2):93–100.
2. Porra RJ, Thompson WA, Kriedemann PE (1989) Determination of accurate extinction coefficients and simultaneous equations for assaying chlorophylls a and b extracted with four different solvents: verification of the concentration of chlorophyll standards by atomic absorption spectroscopy. *Biochim Biophys Acta - Bioenerg* 975(3):384–394.
3. Kato Y, Nagao R, Noguchi T (2016) Redox potential of the terminal quinone electron acceptor QB in photosystem II reveals the mechanism of electron transfer regulation. *Proc Natl Acad Sci* 113(3):620–625.
4. Michaelis L (1932) Theory of the reversible two-step oxidation. *J Biol Chem* 96(3):703–715.
5. Nitschke W (2016) 2-electron redox chemistry. Available at: <http://bip.cnrs-mrs.fr/bip09/2electron.html>.
6. Corrie AR, Nugent JHA, Evans MCW (1991) Identification of EPR signals from the states QaQb and Qb in photosystem II from *Phormidium laminosum*. *Biochim Biophys Acta* 1057(3):384–390.
7. Rutherford AW, Evans MCW (1980) Direct measurement of the redox potential of the primary and secondary quinone electron acceptors in *Rhodospseudomonas sphaeroides* (wild-type) by EPR Spectrometry. *FEBS Lett* 110(2):257–261.
8. Rutherford AW, Heathcote P, Evans MCW (1979) Electron-paramagnetic-resonance measurements of the electron-transfer components of the reaction centre of *Rhodospseudomonas viridis*. Oxidation–reduction potentials and interactions of the electron acceptors. *Biochem J* 182(2):515–523.
9. Heathcote P, Rutherford AW (1986) An EPR Signal Arising from QB-Fe in *Chromatium vinosum*. *Progress in Photosynthesis Research Vol.1* (Dordrecht), pp 201–204.
10. Brudvig GW, Casey JL, Sauer K (1983) The effect of temperature on the formation and decay of the multiline EPR signal species associated with photosynthetic oxygen evolution. *Biochim Biophys Acta - Bioenerg* 723(3):366–371.
11. Rappaport F, Lavergne J (2009) Thermoluminescence: theory. *Photosynth Res* 101(2–3):205–216.
12. Kato Y, et al. (2012) Influence of the PsbA1/PsbA3, Ca(2+)/Sr(2+) and Cl(-)/Br(-) exchanges on

- the redox potential of the primary quinone Q(A) in Photosystem II from *Thermosynechococcus elongatus* as revealed by spectroelectrochemistry. *Biochim Biophys Acta* 1817(11):1998–2004.
13. Vass I, Inoue Y (1986) pH dependent stabilization of S2QA- and S2QB- charge pairs studied by thermoluminescence. *Photosynth Res* 10(3):431–436.
 14. Sugiura M, et al. (2010) Energetics in Photosystem II from *Thermosynechococcus elongatus* with a D1 protein encoded by either the psbA1 or psbA3 gene. *Biochim Biophys Acta - Bioenerg* 1797(8):1491–1499.
 15. Robinson HH, Crofts AR (1983) Kinetics of the oxidation—reduction reactions of the photosystem II quinone acceptor complex, and the pathway for deactivation. *FEBS Lett* 153(1):221–226.
 16. Petrouleas V, Crofts AR (2005) The iron-quinone acceptor complex. *Photosystem II*, eds Wydrzynski T, Satoh K, Freeman J (Springer-Verlag, Berlin/Heidelberg), pp 177–206.
 17. Diner BA (1977) Dependence of the deactivation reactions of Photosystem II on the redox state of plastoquinone pool a varied under anaerobic conditions. Equilibria on the acceptor side of Photosystem II. *BBA - Bioenerg* 460(2):247–258.
 18. Lavergne JJ (1982) Mode of action of 3-(3,4-dichlorophenyl)-1,1-dimethylurea. Evidence that the inhibitor competes with plastoquinone for binding to a common site on the acceptor side of Photosystem II. *BBA - Bioenerg* 682(3):345–353.
 19. Van Best JA, Duysens LNM (1975) Reactions between primary and secondary acceptors of Photosystem II in *Chlorella Pyrenoidosa* under anaerobic conditions as studied by chlorophyll a fluorescence. *BBA - Bioenerg* 408(2):154–163.
 20. Bouges-Bocquet B (1975) Electron Acceptors of Photosystem II. *Proceedings of the 3rd International Congress on Photosynthesis*, ed Avron M (Elsevier), pp 579–588.
 21. Robinson HH, Crofts AR (1984) Kinetics of proton uptake and the oxidation-reduction reactions of the quinone acceptor complex of PS II from pea chloroplasts. *Proc. Intrntl. Cong. Photosynth. Vol I. Brussels, Belgium, Aug 1-6, 1983*, ed Sybesma C (Martinus Nijhoff/Dr. W. Junk, The Hague), pp 477–480.
 22. Graige MS, Feher G, Okamura MY (1998) Conformational gating of the electron transfer reaction QA-.QB --> QAQB-. in bacterial reaction centers of *Rhodobacter sphaeroides* determined by a driving force assay. *Proc Natl Acad Sci U S A* 95(20):11679–84.
 23. Kleinfeld D, Okamura MY, Feher G (1984) Electron-Transfer Kinetics in Photosynthetic Reaction Centers Cooled to Cryogenic Temperatures in the Charge-Separated State: Evidence for Light-Induced Structural Changes. *Biochemistry* 23(24):5780–5786.
 24. Gunner MR, Tiede DM, Prince RC, Dutton PL (1982) Quinones as Prosthetic Groups in Membrane Electron-Transfer Proteins I: Systematic Replacement of the Primary Ubiquinone of Photochemical Reaction Centers wit Other Quinones. *Function of Quinones in Energy Conserving Systems*, ed Trumpower BL (Academic Press), pp 265–269.
 25. Gopher A, et al. (1985) The effect of an applied electric field on the charge recombination kinetics in reaction centers reconstituted in planar lipid bilayers. *Biophys J*. doi:10.1016/S0006-3495(85)83784-X.

26. Garbers A, Reifarh F, Kurreck J, Renger G, Parak F (1998) Correlation between protein flexibility and electron transfer from Q(A)/(-) to Q(B) in PSII membrane fragments from spinach. *Biochemistry* 37(33):11399–11404.
27. Reifarh F, Renger G (1998) Indirect evidence for structural changes coupled with Q(B/-) formation in photosystem II. *FEBS Lett* 428(3):123–126.
28. Fufezan C, Zhang C, Krieger-Liszkay A, Rutherford AW (2005) Secondary quinone in photosystem II of *Thermosynechococcus elongatus*: Semiquinone-iron EPR signals and temperature dependence of electron transfer. *Biochemistry* 44(38):12780–12789.
29. Müh F, Glöckner C, Hellmich J, Zouni A (2012) Light-induced quinone reduction in photosystem II. *Biochim Biophys Acta (BBA)-Bioenergetics* 1817(1):44–65.
30. Cardona T, Sedoud A, Cox N, Rutherford AW (2012) Charge separation in photosystem II: a comparative and evolutionary overview. *Biochim Biophys Acta* 1817(1):26–43.
31. Saito K, Rutherford AW, Ishikita H (2013) Mechanism of proton-coupled quinone reduction in Photosystem II. *Proc Natl Acad Sci* 110(3):954–959.
32. Krieger-Liszkay A, Rutherford AW (1998) Influence of herbicide binding on the redox potential of the quinone acceptor in photosystem II: relevance to photodamage and phytotoxicity. *Biochemistry* 37(50):17339–44.
33. Krieger A, Rutherford AW, Johnson GN (1995) On the determination of redox midpoint potential of the primary quinone electron acceptor, QA, in Photosystem II. *BBA - Bioenerg* 1229(2):193–201.
34. Kern J, et al. (2005) Purification, characterisation and crystallisation of photosystem II from *Thermosynechococcus elongatus* cultivated in a new type of photobioreactor. *Biochim Biophys Acta - Bioenerg* 1706(1–2):147–157.
35. Krivanek R, Kern J, Zouni A, Dau H, Haumann M (2007) Spare quinones in the QB cavity of crystallized photosystem II from *Thermosynechococcus elongatus*. *Biochim Biophys Acta - Bioenerg* 1767(6):520–527.
36. Golbeck JH, Kok B (1979) Redox titration of electron acceptor Q and the plastoquinone pool in Photosystem II. *BBA - Bioenerg* 547(2):347–360.
37. Rich PR, Bendall DS (1980) The kinetics and thermodynamics of the reduction of cytochrome c by substituted p-benzoquinols in solution. *Biochim Biophys Acta - Bioenerg* 592(3):506–518.
38. Zhu Z, Gunner MR (2005) Energetics of quinone-dependent electron and proton transfers in *Rhodobacter sphaeroides* photosynthetic reaction centers. *Biochemistry* 44(1):82–96.
39. Ishikita, H. and Knapp, E.-W. (2003) Redox potential of quinones in both electron transfer branches of photosystem I. *J. Biol. Chem.* 278, 52002– 52011
40. van Mieghem, F., Nitschke, W., Mathis, P. and Rutherford A. W. (1989) The influence of the quinone-iron electron acceptor complex on the reaction centre photochemistry of PS II. *Biochim. Biophys. Acta* 977, 207-214.
41. Kawashima K and Ishikita H. (2017) The influence of the quinone-iron electron acceptor complex on the reaction centre photochemistry of PS II. *Biochemistry* 56, 3019–3028